ARTICLE

B cell-mediated CD4 T-cell costimulation via CD86 exacerbates pro-inflammatory cytokine production during autoimmune intestinal inflammation

Iana Gadjalova [1,2,#], Julia M. Heinze [1,2,#], Marie C. Goess [1,2], Julian Hofmann [1,2,†], Annalisa Buck [3], Marie-Christin Weber [3], Birgit Blissenbach [4], Maximilian Kampick [1,2,‡], Oleg Krut [4], Katja Steiger [5], Klaus-Peter Janssen [3], Philipp-Alexander Neumann [3], Jürgen Ruland [1,2,6,7] and Selina J. Keppler [1,2,8,✉]

Dysregulated B cell responses have been described in inflammatory bowel disease (IBD) patients; however, the role of B cells in IBD pathology remained incompletely understood. We here provide evidence for the detrimental role of activated B cells during the onset of autoimmune intestinal inflammation. Using Wiskott-Aldrich Syndrome interacting protein deficient (*Wipf1*$^{-/-}$) mice as a mouse model of chronic colitis, we identified clusters of differentiation (CD)86 expression on activated B cells as a crucial factor exacerbating pro-inflammatory cytokine production of intestinal CD4 T cells. Depleting B cells through anti-CD20 antibody treatment or blocking costimulatory signals mediated by CD86 through cytotoxic T lymphocyte antigen-4-immunoglobulin (CTLA-4-Ig) diminished intestinal inflammation in our mouse model of chronic IBD at the onset of disease. This was due to a reduction in aberrant humoral immune responses and reduced CD4 T cell pro-inflammatory cytokine production, especially interferon-g (IFN-g) and granulocyte-macrophage colony-stimulating factor (GM-CSF). Interestingly, in addition to B cells isolated from the inflamed colon of *Wipf1*$^{-/-}$ mice, we also found CD86 mRNA and protein expression upregulated on activated B cells isolated from inflamed tissue of human patients with IBD. B cell activation and CD86 expression were boosted by soluble CD40L *in vitro*, which we found in the serum of mice and human patients with IBD. In summary, our data provides detailed insight into the contribution of B cells to intestinal inflammation, with implications for the treatment of IBD.

Mucosal Immunology (2024) 17:67–80; https://doi.org/10.1016/j.mucimm.2023.10.005

INTRODUCTION

Inflammatory bowel disease (IBD), including Crohn's disease and ulcerative colitis (UC), is a group of immune-mediated disorders of the intestine with increasing incidence worldwide[1]. Susceptibility to IBD is driven by environmental risk factors together with a genetic predisposition to aberrant mucosal responses to commensals. Recent single-cell RNA sequencing studies revealed perturbations in humoral immunity during IBD, including the accumulation of B cells, an IBD-specific subset of T follicular helper (TfH) cells, and immunoglobulin (Ig)G plasma cells (PC) in mucosal tissue[2,3]. Furthermore, B cell transcriptomic signatures were enriched in patients with UC refractory to biological therapies[4]. Despite this evidence for a potential implication of B cells in the pathology of IBD, B cell depletion in patients with UC using anti-clusters of differentiation (CD)20 antibodies (rituximab) has shown no benefit[5]. On the contrary, rituximab treatment of patients with extraintestinal inflammatory diseases correlated with colitis-like manifestations; suggesting a protective role for B cells in the gut[6]. Consequently, the potential detrimental or beneficial role of B cells in IBD pathology remains incompletely understood.

B cells might influence intestinal inflammation through antibody and cytokine production or interaction with T cells. In the intestine, activation of B cells takes place in mesenteric lymph nodes (mLN), Peyer's Patches (PP), and isolated lymphoid follicles (ILF) of the lamina propria (LP) and occurs via both T-independent and T-dependent (TD) pathways. T-independent responses potentially involve the recognition of microbial components prevalent in the gut such as lipopolysaccharide (LPS) through Toll-like receptor (TLR)4 expressed on B cells. TD

[#] Both authors equally contributed.
[†] Current affiliation: Turku Bioscience Centre, University of Turku and bo Akademi University, Turku, Finland.
[‡] Current affiliation: Institute of Molecular Immunology, Technical University of Munich, School of Medicine, Munich, Germany.

[1]Institute for Clinical Chemistry and Pathobiochemistry, Technical University of Munich, School of Medicine, Munich, Germany. [2]TranslaTUM, Center for Translational Cancer Research, Technical University Munich, Munich, Germany. [3]Department of Surgery, Technical University of Munich, School of Medicine, Munich, Germany. [4]Paul-Ehrlich-Institut, Langen, Germany. [5]Comparative Experimental Pathology, Institute of Pathology, School of Medicine, Technical University of Munich, Munich, Germany. [6]German Cancer Consortium (DKTK), Heidelberg, Germany. [7]German Center for Infection Research (DZIF), Munich, Germany. [8]Division of Rheumatology and Clinical Immunology, Medical University Graz, Graz, Austria. ✉email: selina.keppler@medunigraz.at

Received: 23 February 2023 Accepted 25 October 2023
Published online: 31 October 2023

responses require signals from CD4 TfH cells[7], which provide costimulatory signals for B cell differentiation and class-switch recombination (CSR) via ligands that include CD40L[8]. During inflammation, exaggerated immune reactions to the microbiota involve a TD response, leading to antibodies of IgA as well as IgG isotypes[9].

A large genome-wide association study among patients with IBD identified over 163 loci associated with IBD risk[10]. A network analysis including these risk loci as well as gene expression data, identified an IBD subnetwork that contains several genes—among them the gene encoding for the actin cytoskeleton regulator Wiskott-Aldrich Syndrome protein (WASp). WAS is an X-linked immunodeficiency associated with an increased susceptibility to infections and autoimmune manifestations. In total, 10% of WAS patients develop early-onset IBD[11], accompanied by systemic autoimmunity[12]. Causes of disease are defective expression of the WASp or the WASp interacting protein (WIP), both regulators of the actin cytoskeleton. WASp as well as WIP-deficient (*Wipf1*$^{-/-}$) mice develop IBD with 100% penetrance[13,14]. We here describe *Wipf1*$^{-/-}$ mice as mouse model of chronic colitis with characteristic immunological features of human IBD and used these mice to test treatment options targeting B cells during IBD.

Our data provides evidence for the detrimental role of B cells during the onset of intestinal inflammation. Using our mouse model of chronic colitis, B cell depletion, mixed bone marrow (BM) chimeric mice, as well as a T cell transfer model of colitis, we identified CD86 expression on activated B cells as crucial factor exacerbating pro-inflammatory cytokine production of CD4 T cells. Depleting B cells or blocking costimulatory signals mediated by CD86 diminished intestinal inflammation in our mouse model of chronic IBD. We also found CD86 messenger RNA (mRNA) and protein expression upregulated on B cells isolated from inflamed tissue of human patients with IBD. Furthermore, we provide evidence that B cell activation and costimulatory molecule expression can be helped additionally by sCD40L present in mouse and human IBD. Collectively, we present evidence for B cells as early drivers of IBD pathogenesis.

RESULTS

Aberrant colonic humoral B cell response in *Wipf1*$^{-/-}$ mice during intestinal inflammation

Wipf1$^{-/-}$ mice developed signs of intestinal inflammation as early as 8 weeks of age, as apparent by a lengthening and thickening of the colon, which resulted in an increased weight-to-length ratio of the colon of *Wipf1*$^{-/-}$ mice compared to littermate controls (Figs 1A and 1B). Furthermore, *Wipf1*$^{-/-}$ mice demonstrated lymphadenopathy in colon draining mLN (colonic mLN, the first and last node of the mLN chain[15]) and enlarged spleens (Supplementary Fig. 1A). Characterizing hallmarks of intestinal inflammation in *Wipf1*$^{-/-}$ mice in detail, we found cell infiltration into the mucosa and submucosa, concomitant with the appearance of neutrophils and mast cells; a thickening of the muscularis interna as well as irregular crypts with increased crypt length, crypt abscesses and goblet cell loss, which resulted in a colitis score with mild to moderate severity (Figs 1C–F, Supplementary Table 1[16]). In addition, we detected a tendency of increased relative mRNA expression of the pro-inflammatory cytokines interleukin (IL)-6 and IL-17A in the inflamed colonic LP of *Wipf1*$^{-/-}$ mice (Supplementary Fig. 1B), concomitant with elevated secretion of these cytokines into the supernatant of cultured intestinal tissue pieces of *Wipf1*$^{-/-}$ mice (Supplementary Fig. 1C).

To determine whether intestinal inflammation in *Wipf1*$^{-/-}$ mice resulted in microbial dysbiosis, we performed 16S ribosomal RNA sequencing on total bacteria isolated from cecal content. Strikingly, while younger (<9 weeks) *Wipf1*$^{-/-}$ mice showed similar bacterial diversity compared to controls, we observed a reduced alpha diversity (Shannon index) in older (>11 weeks) *Wipf1*$^{-/-}$ mice compared to age-matched controls (Supplementary Fig. 1D). Younger *Wipf1*$^{-/-}$ mice demonstrated similar microbial composition compared to wild type (WT) controls (Jaccard distance), whereas older *Wipf1*$^{-/-}$ mice differed significantly (Supplementary Figs. 1E–I) and contained relatively less *Lachnospiracea* and relatively more *Lactobacillacea* (Supplementary Figs. 1G–I). *Wipf1*$^{-/-}$ mice hence demonstrated characteristic features of colonic inflammation.

Next, to assess the recruitment and activation of immune cells to the site of inflammation, we isolated lymphocytes from colonic tissue and analyzed these cells for the protein expression of several lineage- and activation-associated surface markers as well as transcription factors using mass cytometry. Although *ex vivo* isolated total cell numbers from colons of *Wipf1*$^{-/-}$ mice were slightly decreased compared to WT controls (Supplementary Fig. 1J), we found an overabundant population of innate immune cells (monocytes/macrophages) as well as an increased population of IgA PC in lymphocytes isolated from the colonic LP (Supplementary Figs. 1K–N). We next characterized CD4 T cell subsets in the colonic LP of *Wipf1*$^{-/-}$ mice by re-clustering the mass cytometric dataset (Fig. 1G-J). We found an increased population of activated CD4 T cells expressing CD44 isolated from the colonic LP of *Wipf1*$^{-/-}$ mice (about 70% CD44+ CD4 T cells) compared to T cells isolated from WT colonic LP (about 30% CD44+ CD4 T cells) (Fig. 1I). Of these activated CD4 T cells, the frequency of FoxP3 expressing, regulatory CD4 T cells were similar between WT and *Wipf1*$^{-/-}$ mice (Fig. 1J). However, 45% of *Wipf1*$^{-/-}$ activate CD4 T cells expressed the transcription factor IRF4 compared to 20% of WT CD4 T cells, indicating a TfH cell phenotype (Fig. 1J). Concomitantly, using flow cytometry, we also found a 3-fold increase in the frequency of germinal center (GC) B cells expressing GL-7 (T- and B-cell activation marker) and CD95 in lymphocytes isolated from the *Wipf1*$^{-/-}$ colonic LP compared to WT controls (Figs 1K and 1L, Supplementary Fig. 2A), while *ex vivo* isolated, colonic frequencies of CD19 B cells were similar (Supplementary Fig. 2B). These results suggest an ongoing TD immune response in inflamed colonic LP of *Wipf1*$^{-/-}$ mice.

To identify the location and environment of B and T cells infiltrating the inflamed colonic LP in more detail, we used immunofluorescence as well as immunohistochemistry of colonic swiss rolls. We observed large B cell-containing ILFs in the colon of *Wipf1*$^{-/-}$ mice that were rarely detected in littermate controls (Figs 1M–O). These follicles also contained T cells (Fig. 1O). Collectively, enhanced TfH cell numbers, GC B cell responses, and lymphoid follicles in the inflamed colonic LP of *Wipf1*$^{-/-}$ mice demonstrated an ongoing TD immune response.

TD immune responses will lead to CSR and differentiation of B cells to PC. We indeed observed a significant increase in the frequencies of IgA and IgG1 PC in the colon and mLN of *Wipf1*$^{-/-}$ mice (Figs 1P and 1Q, Supplementary Figs. 2C and 2D) using flow cytometry. Analyzing intestinal antibodies, we additionally found increased amounts of intestinal IgA, IgG1, and IgM antibodies using enzyme-linked immunosorbent assay (ELISA) (Supplementary Figs. 2E and 2F).

LPS is prevalent in intestinal tissue and consequently, LPS might be one driver of aberrant colonic humoral responses.

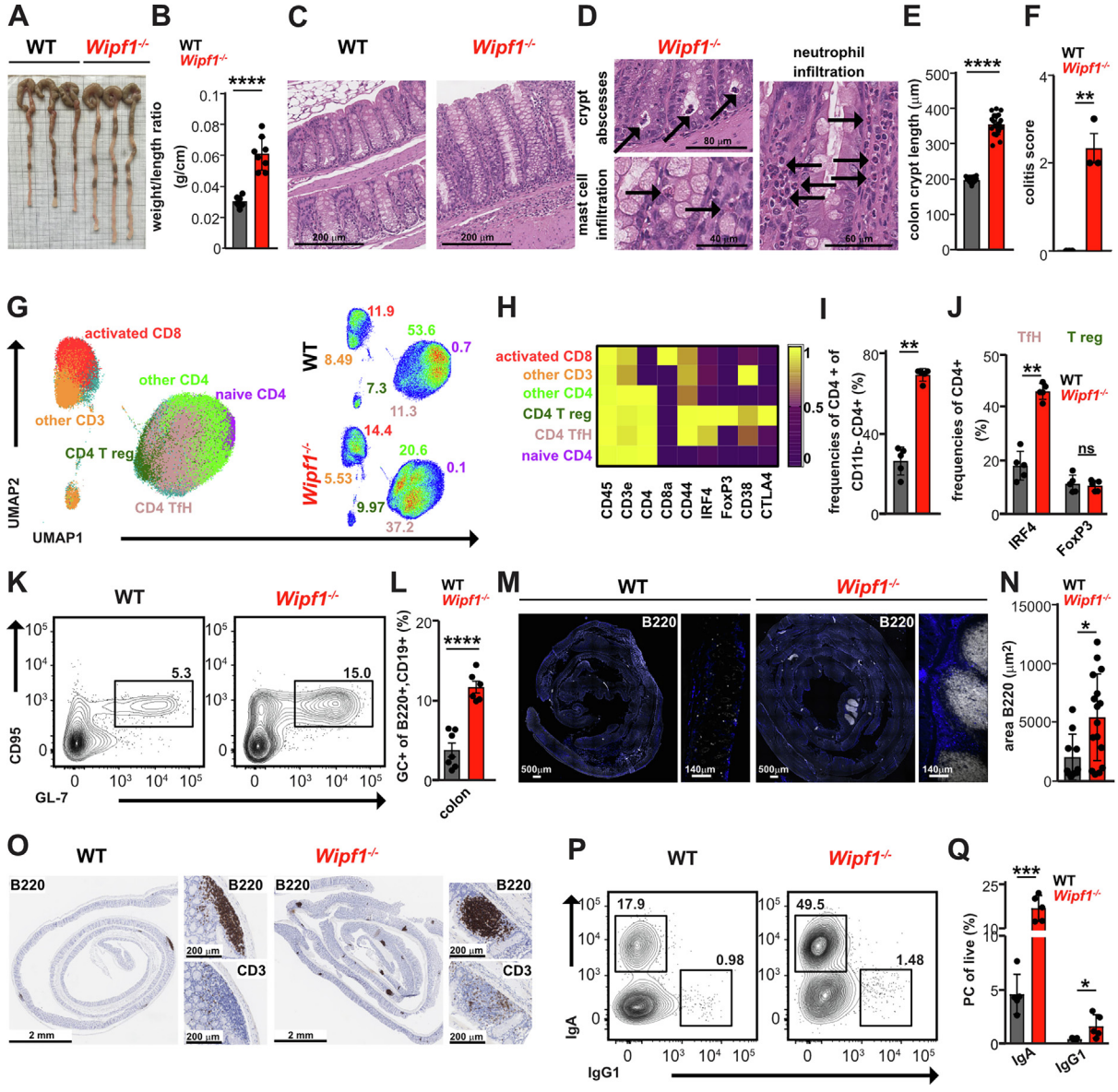

Fig. 1 Aberrant colonic humoral B cell response in Wipf1$^{-/-}$ mice during intestinal inflammation. (A) Representative pictures of cecum and colon isolated from 3 WT and 3 Wipf1$^{-/-}$ mice. (B) Length and weight of the colon was measured and weight to length ratio calculated (n = 8 per genotype, pooled from 4 independent experiments, mean ± SD) Statistical significance was calculated using student's t test. (C) Representative pictures of colonic sections of WT or Wipf1$^{-/-}$ mice stained for H&E <scale bar 200 µm>. (D) Arrows in zoom-ins of colonic sections as in Fig. 1A of Wipf1$^{-/-}$ mice demonstrate crypt abscesses <scale bar 80 µm>, mast cell infiltration <scale bar 40 µm> and neutrophil infiltration <scale bar 60 µm>. (E) Colonic crypt length measured from sections stained with H&E (total of three images, 20 crypts each, mean ± SD). Statistical significance was calculated using student's t test. (F) Colonic inflammation in Wipf1$^{-/-}$ mice was scored according to Table S1[16]. (G) Lymphocytes isolated from colonic tissue of WT or Wipf1$^{-/-}$ mice were analyzed by mass cytometry (n = 5 per genotype, pooled from two independent experiments). UMAP was used to depict CD45 and CD3 expressing T-cell population. FlowSOM-based immune cell populations are overlaid as color dimension. (H) Mean population expression levels of T cell markers used for UMAP visualization and FlowSOM clustering. Frequencies of (I) activated CD4 T cells and (J) IRF4+ T follicular helper or FoxP3+ regulatory T cells (n = 5 per genotype, pooled from two independent experiments). Statistical significance was calculated using Mann-Whitney U-test. (K+L) Lymphocytes isolated from colonic tissue of WT or Wipf1$^{-/-}$ mice were stained to determine germinal center B cells (GC B cells; B220+GL7+CD95+). (K) Representative flow plots of GC B cells (L) Frequencies of GC B cells of total B cells from colonic tissue (n ≥ 6 per genotype, pooled from at least three independent experiments, mean ± SEM). Statistical significance was calculated using student's t test. (M) B220 was stained in complete colonic swiss rolls (zoom-ins on the right, respectively). (N) Quantification of the total area of B220 determined using FIJI. Each dot represents one B cell follicle. Colonic swiss rolls of four animals per genotype were analyzed. Statistical significance was calculated using student's t test. (O) Immunohistochemistry of sections of colonic swiss rolls stained for B220. Zoom-ins of isolated lymphoid follicles (ILFs) indicating B220 as well as CD3 staining. (P+Q) Lymphocytes isolated from colonic tissue were stained to determine PC using flow cytometry (P) Representative flow plots of IgG1 or IgA expressing PC (Q) Frequencies of PC of total live cells from colonic tissue (n ≥ 5 per genotype, pooled from two independent experiments, mean ± SEM) Statistical significance was calculated using Mann-Whitney U-test. *p < 0.05, **p < 0.01, ***p < 0.001, ****p < 0.0001, ns = not significant. CD = clusters of differentiation; H&E = hematoxylin and eosin; PC = plasma cells; Treg = regulatory T cell; Wipf1$^{-/-}$ = Wiskott-Aldrich Syndrome interacting protein deficient; WT = wild type.

Our previous work demonstrated that *Wipf1*$^{-/-}$ B cells are hyperproliferative toward LPS stimulation *in vitro*[17]. We next treated *Wipf1*$^{-/-}$ mice with antibiotics to reduce the microbiome at 6 weeks of age and thus before the onset of intestinal inflammation and before the microbial dysbiosis occurred (Supplementary Figs. 1D, 2G, and 2H). We found a reduced weight-to-length ratio of the colon of treated *Wipf1*$^{-/-}$ mice compared to littermate controls (Supplementary Fig. 2I). Furthermore, we found diminished aberrant humoral immune responses, as measured by a slight reduction of colonic B cell infiltration as well as GC and PC formation, resulting in significantly reduced intestinal antibodies in the colonic tissue of *Wipf1*$^{-/-}$ mice (Supplementary Figs. 2J–N). Together these data indeed point to a crucial role for the microbiome in triggering inflammation and aberrant humoral immune responses in *Wipf1*$^{-/-}$ mice.

Collectively, these findings suggest an aberrant colonic humoral B cell response in *Wipf1*$^{-/-}$ mice, with enhanced infiltration of lymphocytes, GC responses, and TfH cell differentiation in the colonic LP and an aberrant production of intestinal IgG1—all features prevalent also in the inflamed intestinal tissue of patients with IBD[2,3].

Wipf1$^{-/-}$ B cells boost pro-inflammatory cytokine secretion by intestinal CD4 T cells

Activated CD4 T cells in the LP produce pro-inflammatory cytokines, such as granulocyte-macrophage colony-stimulating factor (GM-CSF), IL-6, tumor necrosis factor-alpha (TNF-α), IL-17 and IFN-g, which contribute to disease pathogenesis during intestinal inflammation[18–20]. Considering the increase of activated CD44 expressing CD4 T cells in the LP of *Wipf1*$^{-/-}$ mice, we next assessed the production of pro-inflammatory cytokines by intracellular staining and flow cytometry of re-stimulated colonic CD4 T cells. We found an enhanced frequency of CD4 T cells producing GM-CSF, IFN-g, IL-17A, or IL-17F isolated from the inflamed colonic LP of *Wipf1*$^{-/-}$ mice compared to littermate controls (Figs. 2A–C, Supplementary Figs 3A–C). Similarly, we detected enhanced frequencies of CD44^{+} activated CD4 T cells (Supplementary Fig. 3D) producing pro-inflammatory cytokines (Supplementary Figs. 3E and 3F) in the intestinal draining mLN of *Wipf1*$^{-/-}$ mice compared to their WT counterparts. Of note, CD4 T cells coexpressing IFN-g and GM-CSF or IL-17A and IL-17F were detectable in the colonic LP and mLN of *Wipf1*$^{-/-}$ mice only (Figs. 2B and 2C, Supplementary Figs. 3B, 3C, 3E, and 3F). Together these findings showed that CD4 T cells produce colitis-associated inflammatory cytokines characteristic of the pro-inflammatory T helper (TH)1/TH17 T cell subsets in the inflamed colonic tissue of *Wipf1*$^{-/-}$ mice.

Given the substantial infiltration of B cells into the inflamed colonic LP of *Wipf1*$^{-/-}$ mice, and the observed TD immune response suggesting the interaction of B and T cells, we next assessed the role of B cells in CD4 T cell cytokine production during intestinal inflammation. For this, we depleted B cells of *Wipf1*$^{-/-}$ mice at 6 and 8 weeks of age and hence before the manifestation of colonic inflammation using an anti-CD20 antibody (Fig. 2D). B cell depletion did not affect the body weight or the colonic weight-to-length ratio of *Wipf1*$^{-/-}$ mice compared to control mice (Supplementary Figs. 4A and 4B). B cells were efficiently depleted in the spleen and mLN (Supplementary Figs. 4C and 4D), which resulted in a 50% reduction of total lymphocyte numbers in mLN of *Wipf1*$^{-/-}$ mice (Supplementary Fig. 4E). We found incomplete depletion of B cells in PP, colon as well as the peritoneal cavity (Supplementary Figs. 4C and 4D). Anti-CD20 treatment of *Wipf1*$^{-/-}$ mice led to a reduction in IgA as well as IgG1 PC numbers in mLN (Supplementary Fig. 4F). Concurrent with the reduced antibody-secreting cells (ASCs), intestinal antibody levels in colonic mucus (Supplementary Fig. 4G) were reduced in anti-CD20 treated *Wipf1*$^{-/-}$ mice. Due to the severely reduced survival of cells isolated from the inflamed colonic tissue of *Wipf1*$^{-/-}$ mice at 10 weeks of age (less than 10% living cells, Supplementary Fig. 4H), we restricted our analyses to lymphocytes isolated from mLNs. Notably, B cell depletion in *Wipf1*$^{-/-}$ mice did not influence the frequencies of CD4 T cells isolated from mLN (Supplementary Fig. 4I) but led to slightly but consistently reduced frequencies of activated CD44^{+} CD4 T cells as well as reduced intracellular IFN-g and IL-17A staining (Figs. 2E–G, Supplementary Fig. 4J) in CD4 T cells isolated from mLN. Thus, B cell depletion during the onset of intestinal inflammation reduced CD4 T cell activation and cytokine production.

To establish whether the absence of WIP exclusively in B cells has an effect on pro-inflammatory cytokine production of colonic T cells, we next generated mixed-BM chimeric mice by adoptively transferring 80% BM from either WT or *Wipf1*$^{-/-}$ mice and 20% BM from mice that lack B cells (JHT mice) into lethally irradiated *Rag1*$^{-/-}$ recipients (Fig. 2H). In this setting, all newly generated B cells will be *Wipf1*$^{-/-}$ in an environment containing mainly WT cells. Ten weeks after adoptive transfer, B cells have repopulated the colonic tissue with a slight reduction in B cells (Supplementary Fig. 4K) as well as IgA PC frequencies (Supplementary Fig. 4L) in JHT-Wipf1$^{-/-}$ chimeric mice compared to controls. Nevertheless, we found increased IgA antibody levels in the mucus in JHT-Wipf1$^{-/-}$ chimeric mice compared to controls (Supplementary Fig. 4M). Strikingly, we detected a pronounced increased frequency of activated CD44^{+} CD4 T cells (Supplementary Fig. 4N) concomitant with enhanced pro-inflammatory cytokine production of CD4 T cells (GM-CSF, IFN-g, IL-17A and IL-17F) isolated from the LP of the inflamed colon of JHT-Wipf1$^{-/-}$ chimeric mice (Figs 2I and 2J).

Collectively, our data provided evidence that *Wipf1*$^{-/-}$ B cells directly promote pro-inflammatory cytokine production of CD4 T cells, thus likely enhancing intestinal inflammation.

Wipf1$^{-/-}$ B cells are sufficient to enhance pro-inflammatory cytokine production in WT CD4 T cells in a T cell transfer colitis model

To address the influence of B cells on CD4 T cell cytokine production in an acute model of colitis in which only B cells lack WIP, we made use of a T-cell transfer colitis model. In this model, the transfer of naive CD4^{+}CD45RB^{high} WT T cells in the absence of T regulatory cells generates large numbers of disease-promoting TH1 and TH17 cells[21]. We cotransferred purified B cells isolated from mLN of WT or *Wipf1*$^{-/-}$ mice together with naive WT T cells into *Rag1*$^{-/-}$ recipients and analyzed lymphocyte populations isolated from colonic tissue or mLN 8 weeks after transfer (Fig. 3A). Weekly scoring of the mice showed a weight gain of *Rag1*$^{-/-}$ recipients which received WT B cells as compared to no B cell transfer, which was reduced if *Wipf1*$^{-/-}$ B cells were transferred (Fig. 3B). Interestingly, transfer of *Wipf1*$^{-/-}$ B cells led to enhanced colonic weight-to-length ratio concomitant with increased total cell numbers isolated from mLN or colonic tissue of *Rag1*$^{-/-}$ recipients, compared to controls (Figs 3C and 3D). We noticed that most of the transferred B cells differentiated into IgA ASCs, with only a modest reduction in total cell numbers and frequencies of IRF4^{+} IgA^{+} CD19^{low}

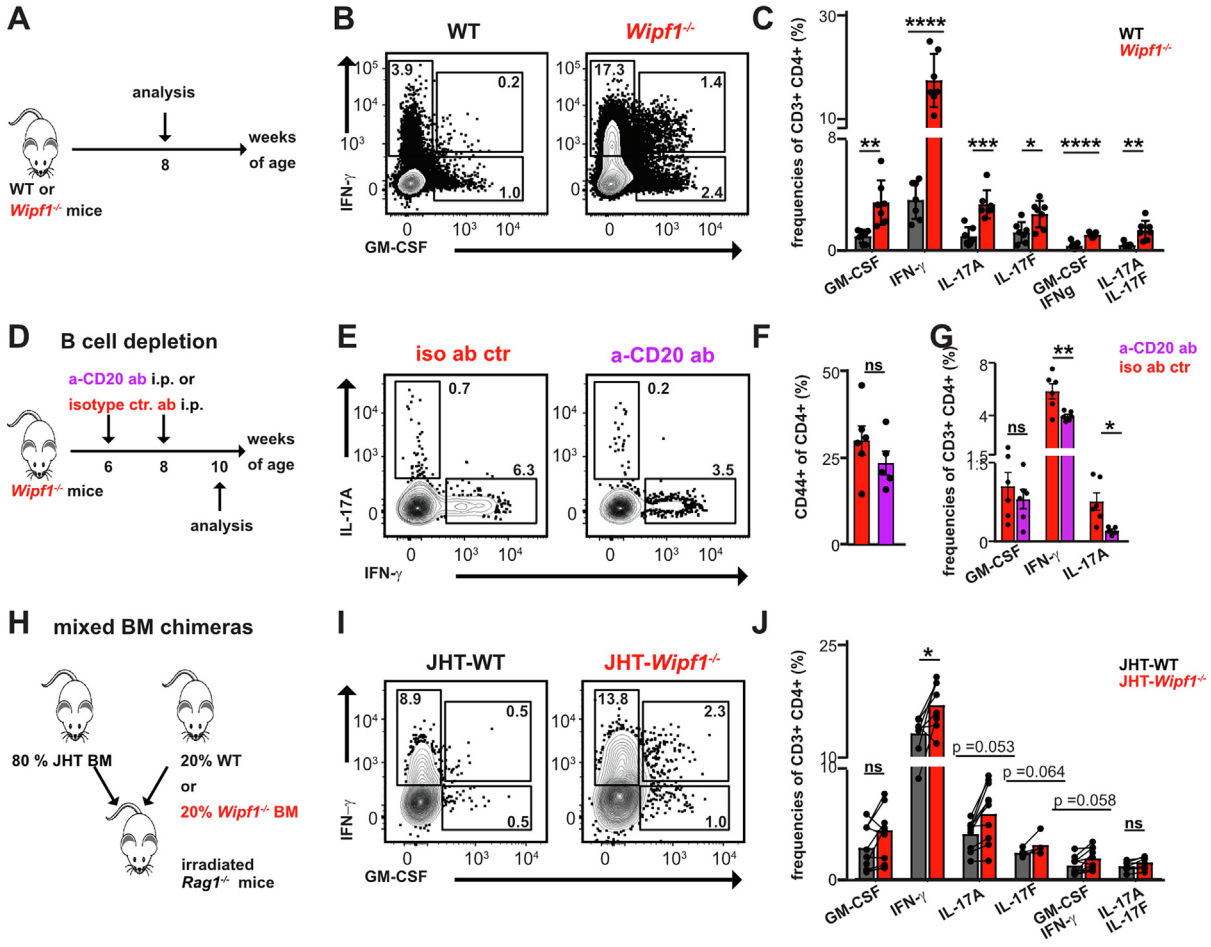

Fig. 2 Wipf1$^{-/-}$ B cells boost pro-inflammatory cytokine secretion by intestinal CD4 T cells. (A) Schematic indicating the time-point of analysis of cytokine production of CD4 T cells isolated from colonic tissue of WT or Wipf1$^{-/-}$ mice. (B+C, E-G, I+J) Lymphocytes were isolated from (B+C, I+J) colonic tissue or (E–G) mLN of (B+C) WT or Wipf1$^{-/-}$ mice, (E–G) Wipf1$^{-/-}$ mice treated with either isotype control antibody or anti-CD20 antibody to deplete B cells, or (I+J) JHT-WT or JHT-Wipf1$^{-/-}$ mixed BM chimeric mice and stimulated with Brefeldin A and PMA/Ionomycin for 4 hours. (B, E, I) Representative flow plots of CD4 T cells intracellularly expressing indicated cytokines. Gating strategy is shown in Fig. S2A. (C, F, J) Frequencies of intracellular staining of indicated cytokines of CD4 T cells after in vitro re-stimulation gated as shown in Fig. S2A. (D) Experimental setup of B cell depletion in Wipf1$^{-/-}$ mice. (G) Frequencies of CD44+ CD4 T cells. (H) Experimental setup of the generation of JHT-WT or JHT-Wipf1$^{-/-}$ mixed bone-marrow (BM) chimeric mice. (A–J) n ≥ 6 mice per genotype, pooled from two to three independent experiments. Statistical significance was calculated using student's t test. *p < 0.05, **p < 0.01, ***p < 0.001, ****p < 0.0001. BM = bone marrow; CD = clusters of differentiation; Ig = immunoglobulin; ns = not significant; PMA = Phorbol myristate acetate; Wipf1$^{-/-}$ = Wiskott-Aldrich Syndrome interacting protein deficient; WT = wild type.

Wipf1$^{-/-}$ cells isolated from colonic tissue (Figs 3E–G, Supplementary Figs. 5A–C). This decrease was reflected in reduced levels of IgA antibodies detected in the mucus of recipients who received *Wipf1*$^{-/-}$ B cell (Supplementary Fig. 5D). Interestingly, in *Wipf1*$^{-/-}$ B cell cotransferred recipients, numbers, and frequencies of total CD4 T cells as well as activated CD44^{+} CD4 T cells were slightly increased in cells isolated from the mLN and colon (Supplementary Figs. 5E–H). Strikingly, CD4 T cells isolated from mLN of *Wipf1*$^{-/-}$ B cell transferred mice demonstrated significantly enhanced numbers and a modest increase in frequencies of pro-inflammatory cytokine-expressing cells (Figs 3H and 3I, Supplementary Figs. 5I and 5J). This was less apparent in CD4 T cells isolated from colonic tissue, most likely due to the strong acute inflammation in the colonic LP of all recipient mice (Supplementary Figs. 5K–M). Together, these results again reinforce a role for *Wipf1*$^{-/-}$ B cells in fueling intestinal inflammation through CD4 T-cell activation.

B cell-mediated costimulation via CD86 enhances CD4 T cell pro-inflammatory cytokine production

To get a better insight into how *Wipf1*$^{-/-}$ B cells promote CD4 T cell cytokine production, we used an *in vitro* mixed-lymphocyte reaction to activate T cells by means of MHC-II mismatch. We stimulated purified mLN B cells from WT or *Wipf1*$^{-/-}$ BALB/c mice with LPS and cultured them with naive, splenic CD4 T cells isolated from C57BL/6 mice (Fig. 4A). As both, B and T cells can contribute to cytokine secretion in these cocultures, we measured total cytokines in the culture supernatant using ELISA. We found GM-CSF and IFN-g the most prevalent cytokines secreted into the supernatants of those cocultures (Fig. 4B). B cells contributed to IL-6 and IL-10 cytokine levels in the culture supernatant (Supplementary Fig. 6A). Concomitant with our previous finding that *Wipf1*$^{-/-}$ B cells are hyper-proliferative to LPS stimulation *in vitro*[17], *Wipf1*$^{-/-}$ B cells were more efficient in secreting those cytokines compared to WT B cells (Supplementary Fig. 6A).

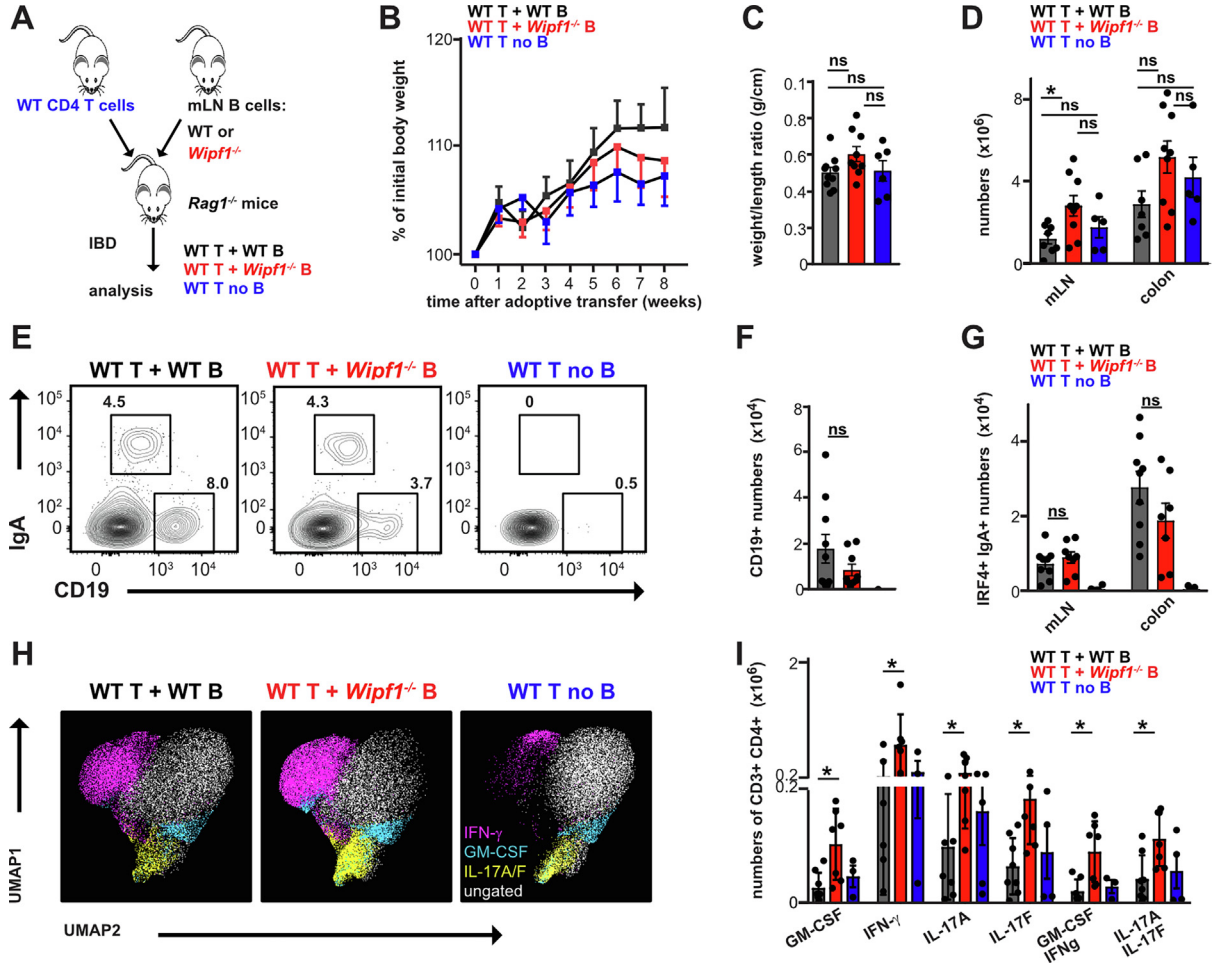

Fig. 3 *Wipf1*$^{-/-}$ B cells are sufficient to enhance pro-inflammatory cytokine production in WT CD4 T cells in a T cell transfer colitis model. (A) Experimental setup of the adoptive transfer of naïve T cells together with WT or *Wipf1*$^{-/-}$ B cells into *Rag1*$^{-/-}$ recipients to induce colitis. (B) Body weights shown as percentage of starting weight. (C) Length and weight of the colon was measured and weight to length ratio calculated. Statistical significance was calculated using Mann-Whitney U-test. (D) Total cell numbers isolated from mLNs or colonic tissue. (E) Representative flow plots of B cells (CD19+) and IgA PC (IgA+,CD19low) isolated from mLNs. (F) Total numbers of B cells isolated from mLNs. (G) Total numbers of IgA+ PC isolated from mLNs or colonic tissue. (H+I) Lymphocytes were isolated from mLNs and stimulated with Brefeldin A and PMA/Ionomycin for 4 hours. (H) UMAP was used to depict cytokine producing CD4 T cells. Manually gated CD4 T cells expressing indicated cytokines are overlaid as color dimension. (I) Total cell numbers of CD4 T cells isolated from mLN expressing indicated cytokines intracellularly after in vitro re-stimulation. (A–I) $n \geq 5$ per genotype, pooled from three independent experiments (all mean +/- SEM). Statistical significance was calculated using ordinary one-way analysis of variance with Tukey's multiple comparison test, or tow-way analysis of variance with Sidak's multiple comparison test. *p < 0.05, **p < 0.01, ***p < 0.001, ****p < 0.0001. CD = clusters of differentiation; Ig = immunoglobulin; ns = not significant; PC = plasma cells; *Wipf1*$^{-/-}$ = Wiskott-Aldrich Syndrome interacting protein deficient; WT = wild type.

Importantly, the concentration of both, GM-CSF and IFN-g, but also TNF-α, IL-6, and IL-10 were significantly increased in the coculture supernatants of WT T/*Wipf1*$^{-/-}$ B cells compared to supernatants of WT T/WT B cell cocultures (Fig. 4B). This was not due to an increase in cell numbers of *Wipf1*$^{-/-}$ B cells, as frequencies were comparable to WT B cells at days 2 and 5 of the coculture (Supplementary Fig. 6B), likely due to the previously reported diminished survival of *Wipf1*$^{-/-}$ B cells[17]. Thus, the presence of *Wipf1*$^{-/-}$ B cells enhanced the secretion of GM-CSF as well as IFN-g of WT CD4 T cells *in vitro* as well as *in vivo*.

B cells interact with T cells by means of costimulatory molecules such as CD86/CD80 engaging CD28 or CD40 engaging CD40L (Fig. 4C). We found that, compared to WT B cells, *Wipf1*$^{-/-}$ B cells expressed higher levels of CD86 on their surface, which is further increased by the presence of T cells (Figs 4D and 4E, Supplementary Figs. 6C and 6D). Enhanced surface expression of CD86 is intrinsic to *Wipf1*$^{-/-}$ B cells as *Wipf1*$^{-/-}$ B cells isolated from JHT-Wipf1$^{-/-}$ chimeric mice demonstrated enhanced CD86 expression compared to JHT-WT B cells in the presence of T cells after LPS stimulation (Supplementary Fig. 6E). In contrast to CD86 surface expression levels, CD80, CD40 and MHC-II expression levels were similar between WT and *Wipf1*$^{-/-}$ B cells at day 2 after LPS stimulation in the presence or absence of T cells (Supplementary Figs. 6F–K). Of note, the expression level of CD86 was boosted further on WT and *Wipf1*$^{-/-}$ B cells by the combined stimulation with CD40L and LPS (Fig. 4F). Furthermore, *Wipf1*$^{-/-}$ B cells are also hyper-proliferative to CD40L stimulation *in vitro*[17], and CD4 T cells provide this costimulatory

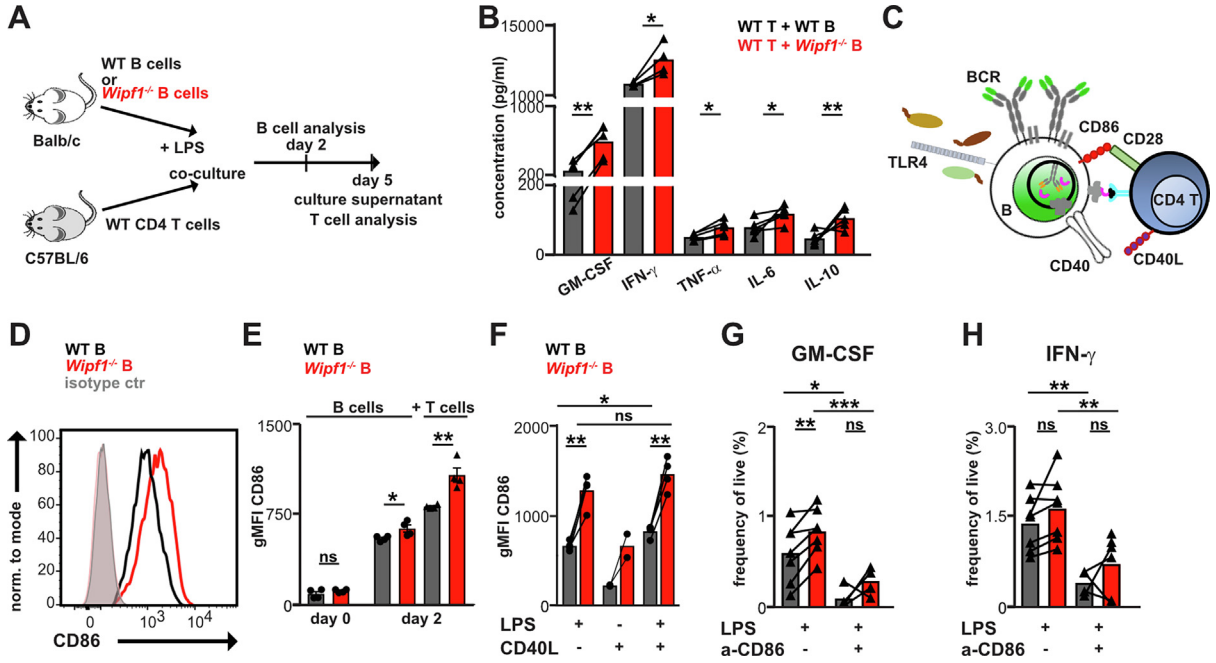

Fig. 4 B cell mediated costimulation via CD86 enhances CD4 T cell cytokine production. (A) Experimental setup of the mixed-lymphocyte reaction. (B) Indicated cytokines secreted into the coculture supernatants were analyzed using a multiplex assay. (C) Schematic indicating herein analyzed surface molecules involved in B/T interactions. (D+E) Flow cytometry analysis of CD86 expression on mLN WT or *Wipf1*$^{-/-}$ B cells stimulated with LPS for 48 hours in the presence of T cells. (D) Representative histogram overlay. (E) CD86 expression quantified by analyzing the gMFI. (F) Flow cytometry analysis of CD86 expression on B cells stimulated for 48 hours with LPS, CD40L or both and quantified by analyzing the gMFI. (G+H) Frequencies of (G) GM-CSF or (H) IFN-γ expressing CD4 T cells stimulated with Brefeldin A for 4 hours, stained and analyzed by flow cytometry at day 5 of coculture. $n \geq 4$ mice per genotype (except CD40L alone $n = 2$), pooled from multiple experiments. Statistical significance was calculated using student's t test. *p < 0.05, **p < 0.01, ***p < 0.001, ****p < 0.0001. CD = clusters of differentiation; GM-CSF = granulocyte-macrophage colony-stimulating factor; gMFI = geometric mean fluorescence intensity; Ig = immunoglobulin; INF = interferon; ns = not significant; PC = plasma cells; *Wipf1*$^{-/-}$ = Wiskott-Aldrich Syndrome interacting protein deficient; WT = wild type.

signal to B cells, thus likely and further enhancing CD86 expression.

Next, we sought to determine the role of CD86 in CD4 T cell cytokine production. Coculturing WT CD4 T with *Wipf1*$^{-/-}$ B cells not only enhanced cytokine secretion into the culture supernatant (Fig. 4B, Supplementary Figs. 6L and 6M), but also elevated the frequencies of cytokine-producing CD4 T cells as measured by intracellular flow cytometry (Figs 4G and 4H, Supplementary Fig. 6O). Blocking B/T interaction by anti-CD86 antibodies reduced the frequencies of cytokine-producing CD4 T cells as well as secreted GM-CSF and IFN-g (Figs 4G and 4H, Supplementary Figs. 6L and 6M), but did not influence B cell survival (Supplementary Fig. 6N). CD80/CD86 costimulatory signals can be inhibited by binding of abatacept[22]. Abatacept is a recombinant fusion protein of the cytotoxic T lymphocyte antigen-4 (CTLA-4) with the Fc portion of human IgG1 (CTLA-4-Ig). Concomitant with the enhanced expression of CD86 48 hours after LPS stimulation *in vitro* (Figs 4D and 4E), staining of *Wipf1*$^{-/-}$ B cells with CTLA-4-Ig demonstrated enhanced binding compared to WT B cells (Supplementary Figs. 6P and 6Q) using flow cytometry. We next tested if CTLA-4-Ig treatment also inhibited naive CD4 T-cell costimulation by binding to CD80/CD86 and thus limited CD4 T cell cytokine production using our *in vitro* assay. We stimulated WT B cells together with naive CD4 T cells in the presence or absence of anti-CD86 blocking antibodies or CTLA-4-Ig. Addition of CTLA-4-Ig to the cocultures indeed reduced the frequencies of IFN-g-producing CD4 T cells similar to adding anti-CD86 antibodies (Supplementary Fig. 6R). These results demonstrated that costimulatory signals via CD80/CD86 can efficiently be blocked *in vitro* by adding CTLA-4-Ig.

Collectively, our findings suggest that B cell-derived costimulation of CD4 T cells via CD86 promotes pro-inflammatory cytokine production of CD4 T cells. Furthermore, cell-intrinsic hyperreactivity of *Wipf1*$^{-/-}$ B cells toward LPS stimulation enhances CD86 expression and hence the costimulatory capacity of *Wipf1*$^{-/-}$ B cells, thereby exacerbating CD4 T cell pro-inflammatory cytokine production.

CTLA-4-Ig treatment is effective in reducing aberrant intestinal humoral immune responses and inflammation

Abatacept is approved for the treatment of rheumatoid arthritis (RA) patients, in which it diminishes plasmablasts and serum IgG[22]. To answer the question if CTLA-4-Ig could be effective in reducing aberrant humoral B cell responses and CD4 T cell cytokines *in vivo*, we first determined the expression of CD86 on B cells isolated from colonic tissue. Consistent with our *in vitro* data, we also observed a higher expression of CD86, but not CD80, on colonic *Wipf1*$^{-/-}$ B cells compared to WT B cells *ex vivo* (Figs 5A and 5B). The expression of both, CD86 and CD80, was similar or even reduced on monocytes isolated from colonic tissue of *Wipf1*$^{-/-}$ compared cells isolated from WT mice (Supplementary Fig. 7A), indicating that CD86 upregulation was specific

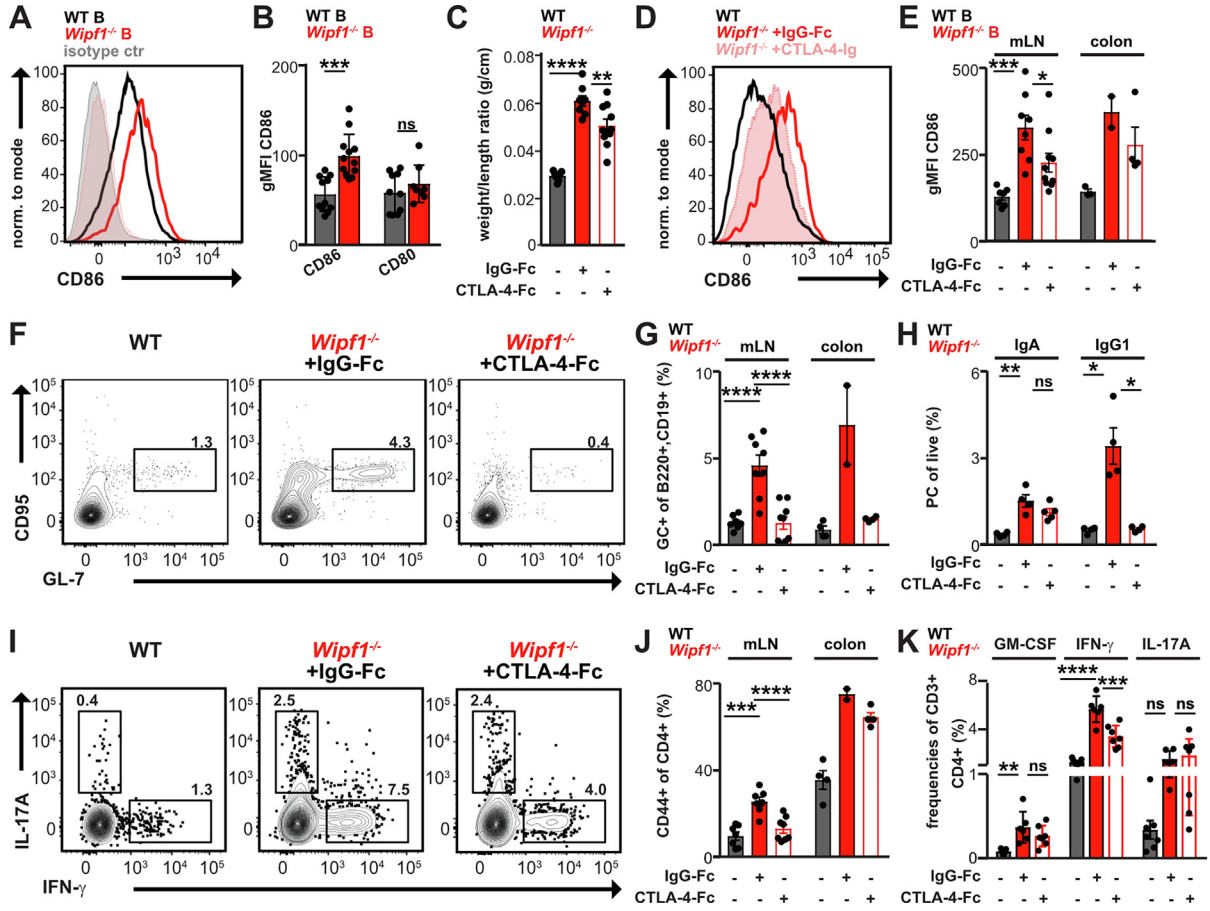

Fig. 5 CTLA-4-Ig treatment is effective in reducing aberrant intestinal humoral immune responses and inflammation. (A) Flow cytometry analysis of CD86 expression on ex vivo isolated colonic B cells of WT or *Wipf1*$^{-/-}$ mice. (B) CD86 and CD80 expression of B cells quantified by analyzing the gMFI. $n \geq 5$ mice per genotype. (C) Length and weight of the colon was measured and weight to length ratio calculated of *Wipf1*$^{-/-}$ mice treated with CTLA-4-Ig or IgG-Fc control compared to untreated WT mice. (D) Flow cytometry analysis of CD86 expression on ex vivo isolated colonic B cells of indicated mice. (E) CD86 expression quantified by analyzing the geometric mean fluorescence intensity (gMFI) in B cells from indicated mice isolated from mLN or colonic tissue. (F) Representative flow plots of GC B cells isolated from mLN of indicated mice. (G) Frequencies of GC B cells of total B cells from mLN or colonic tissue. (H) Frequencies of PC of total live cells isolated mLN or colonic tissue of indicated mice. (I) CD4 T cells isolated from mLN of WT or *Wipf1*$^{-/-}$ mice treated with either CTLA-4-Ig or IgG-Fc control were stimulated with Brefeldin A and PMA/Ionomycin for 4 hours. Representative flow plots of CD4 T cells intracellularly expressing indicated cytokines. (J) Frequencies of CD44+ CD4 T cells. (K) Frequencies of intracellular staining of indicated cytokines of CD4 T cells after in vitro re-stimulation ($n = 4$ per genotype, mean ± SEM). Statistical significance was calculated using ordinary one-way or two-way analysis of variance with Tukey's multiple comparison test. *p < 0.05, **p < 0.01, ***p < 0.001, ****p < 0.0001. CD = clusters of differentiation; CTLA-4 = cytotoxic T lymphocyte antigen-4; GC = germinal center; gMFI = geometric mean fluorescence intensity; Ig = immunoglobulin; mLN = mesenteric lymph nodes; ns = not significant; PC = plasma cells; *Wipf1*$^{-/-}$ = Wiskott-Aldrich Syndrome interacting protein deficient; WT = wild type.

to *Wipf1*$^{-/-}$ B cells. We next treated *Wipf1*$^{-/-}$ mice with CTLA-4-Ig or control IgG-Fc twice at disease onset and compared these mice with untreated WT littermate controls (Supplementary Fig. 7B). Interestingly, although CTLA-4-Ig or control IgG-Fc treated mice gained similar weight (Supplementary Fig. 7C), the colon weight-to-length ratio was reduced 4 weeks after the first treatment (Fig. 5C). We again noticed a severely reduced survival of cells isolated from the inflamed colonic tissue of *Wipf1*$^{-/-}$ mice at 10 weeks of age, which was greatly enhanced after CTLA-4-Ig treatment, hinting at lowered intestinal inflammation (Supplementary Fig. 7D). Furthermore, CTLA-4-Ig treatment significantly reduced CD86 expression on B cells isolated from the colon or mLN of *Wipf1*$^{-/-}$ mice compared to IgG-Fc treated mice (Figs 5D and 5E, Supplementary Fig. 7E). Analyzing TD immune responses in the mLN and colon, we detected substantially decreased frequencies of GC B cells (Figs 5F and 5G, Supplementary Fig. 7F), concomitant with reduced CSR and differentiation of B cells to IgG1 expressing plasmablasts and PC (Fig. 5H, Supplementary Figs 7G and 7H) in CTLA-4-Ig treated *Wipf1*$^{-/-}$ mice compared to IgG-Fc treated mice and comparable to WT littermate controls. Additionally, CTLA-4-Ig treatment significantly reduced frequencies of activated, CD44 expressing as well as IFN-g producing CD4 T cells in the mLN of *Wipf1*$^{-/-}$ mice (Fig. 5 I-K). Together, these results indicate that CTLA-4-Ig treatment at the onset of disease is effective in reducing aberrant intestinal humoral immune responses and inflammation.

B cells in inflamed intestinal tissue of patients with IBD express elevated CD86

LPS is prevalent in the gut and inflammation enhances the dissemination of bacteria into the surrounding tissue[23]. Our *in vitro* data showed that WT B cells in the presence of LPS enhance CD86 expression and thus have enhanced costimulatory properties (Fig. 4E). Blocking of CD86 using anti-CD86 antibodies or CTLA-4-Ig reduced CD4 T cell cytokine production in cocultures with WT B cells *in vitro* (Supplementary Fig. 6R). We hypothesized that in an inflamed environment such as during IBD, activated B cells might enhance surface CD86 expression and thus CD4 T-cell costimulation. Interestingly, concomitant with pronounced B cell infiltration mainly into large ILF-like structures (Figs 6A and 6B, Supplementary Figs. 8A and 8B), CD86 is among the top 100 significantly upregulated genes in GC and follicular B cells in two single-cell RNA sequencing (scRNA-seq) analysis of differentially expressed genes in colonic biopsies of inflamed patients with UC compared to healthy tissue (Fig. 6C, Supplementary Figs. 8C–G and[3,24]). Importantly, we also found CD86 to be increased on B cells isolated from inflamed tissue of patients with IBD compared to B cells isolated from non-involved tissue analyzed on protein level by flow cytometry (Figs 6D and 6E). Hence CD86 expression on B cells might push inflammatory cytokine production in CD4 T cells also in patients with IBD. Our *in vitro* data implied a role for CD40 stimulation by CD40L in boosting CD86 expression on B cells. We indeed found sCD40L to be elevated in both, sera of *Wipf1*$^{-/-}$ mice as well as patients with IBD compared to controls (Figs 6F and 6G).

Collectively the data presented here suggest that upregulation of the costimulatory molecule CD86 plays a crucial role in B/T interaction in inflamed colonic tissue, thereby enhancing aberrant humoral immunity, and priming pro-inflammatory cytokine production in CD4 T cells. Enhanced expression of CD86 on B cells could be boosted by the presence of soluble CD40L in our mouse model of chronic colitis but also in human patients with IBD.

DISCUSSION

Perturbations in humoral immunity have been described during IBD, including the accumulation of intestinal B cells, an IBD-specific subset of TfH cells, and IgG PC in mucosal tissue[2,3]. Despite evidence for a potential implication of B cells in the pathology of IBD, the potential detrimental or beneficial role of B cells in IBD pathology remained incompletely understood. We here provide evidence for the detrimental role of B cells during the onset of intestinal inflammation. We identified CD86 expression on activated B cells as crucial factor exacerbating pro-inflammatory cytokine production (especially IFN-g and GM-CSF) of CD4 T cells. Depleting B cells or blocking costimulatory signals mediated by CD86 through CTLA-4-Ig treatment diminished intestinal inflammation in our mouse model of IBD at the onset of disease. We further found CD86 mRNA and protein expression also upregulated in human patients with IBD and hence provide a possible explanation for the observed aberrant humoral immune response signatures during human IBD[2,3].

Investigating *Wipf1*$^{-/-}$ mice, we found that changes in the fecal microbiome correlated with the onset of disease. While younger *Wipf1*$^{-/-}$ mice demonstrated bacterial diversity similar to that of WT mice, only 2 weeks older *Wipf1*$^{-/-}$ mice demonstrated a reduced microbial diversity characteristic for intestinal inflammation. We found relatively reduced levels of *Lachnospiraceae*, similar to what has been described in CD patients[25]. *Lachnospiraceae* are known to provide short-chain fatty acids, microbial metabolites, which enhance the differentiation of regulatory B and T cells[26,27]. Antibiotic treatment of young *Wipf1*$^{-/-}$ mice diminished the formation of GC and reduced CD4 T-cell activation and IFN-g production. In our study, we cannot resolve the question if an early intestinal barrier breach or the hyperreactivity of *Wipf1*$^{-/-}$ B cells toward the commensal microbiome is the cause or consequence of microbial dysbiosis and intestinal inflammation. Additionally, the absence of regulatory monocytes as demonstrated in WASp-deficient mice[28] might also play a role in dysbiosis and intestinal inflammation in *Wipf1*$^{-/-}$ mice. Future studies should aim to investigate the relationship between aberrant intestinal antibody production on monocyte activation and its role during intestinal inflammation in more detail.

We previously used *Wipf1*$^{-/-}$ mice to investigate the role of the actin cytoskeleton in B cell activation during WAS. Our work demonstrated that WIP functions as a regulator of CD19 activation and phosphoinositide 3-kinase (PI3K)/protein kinase B (Akt) signaling in B cells[17]. *Wipf1*$^{-/-}$ B cells are hyper-proliferative toward LPS and CD40L stimulation[17] and we here showed that both stimuli enhanced CD86 expression *in vitro*. Furthermore, we found that CD4 T cell pro-inflammatory cytokine production, especially GM-CSF and IFN-g, requires CD86 expression on B cells and is proportional to the amount of CD86 expressed. Recent data demonstrated that B cells from lupus-prone mice used CD86 expression together with IL-6 secretion to expand inflammatory TH17 cells *in vitro*[29]. Our *in vitro* and *in vivo* data rather indicate the expansion of IFN-g and GM-CSF-producing TH1-like cells. In addition, *Wipf1*$^{-/-}$ B cells demonstrated enhanced secretion of IL-6 into the culture supernatant after LPS stimulation *in vitro*, the potential role for B cell-derived IL-6 in the polarization of CD4 T cells warrants further investigation.

Our recent data demonstrated that WIP deficiency resulted in defects in B cell homing, chemotaxis, survival, and differentiation, ultimately leading to diminished GC formation and antibody production after vaccination[17]. At the same time, *Wipf1*$^{-/-}$ mice demonstrate features of autoimmunity, such as autoantibody production or the spontaneous formation of GC. Similarly, B cell-intrinsic deletion of WASp in mice is sufficient to result in autoantibody production and the induction of spontaneous GC formation[30–32]. B cell-dependent spontaneous GC formation concomitant with autoantibody production in spleen and lymph nodes have been linked toTLR7 and MyD88 signaling[30,33] as well as B cell-intrinsic IFN-g signaling or IL-6 secretion[34,35]. WASp deletion specifically in GC B cells reduces apoptosis, leading to tolerance loss and the development of autoimmunity[36].

Despite our initial observation of impaired homing of *Wipf1*$^{-/-}$ B cells into the spleen[17], we detected efficient homing of *Wipf1*$^{-/-}$ B cells to intestinal-associated tissues (mLN, PP, colonic tissue) using mixed-BM chimeras (own preliminary data). These findings together with the reduction of aberrant humoral immune responses after antibiotics treatment suggest that homing of *Wipf1*−/− B cells might be influenced by additional stimulatory cues (such as LPS, chemokines) present in the intestine. In this line, during intestinal inflammation, we found a substantial increase in B cell-containing follicles in the inflamed colonic LP in *Wipf1*$^{-/-}$ mice. Enhanced GC formation as well as the presence of IgG1 ASC indicated an ongoing TD immune response. It is tempting to speculate that the ongoing immune response in the intestine, especially during inflammation, might trigger tolerance loss in hyper-reactive *Wipf1*$^{-/-}$ B cells, eventually leading

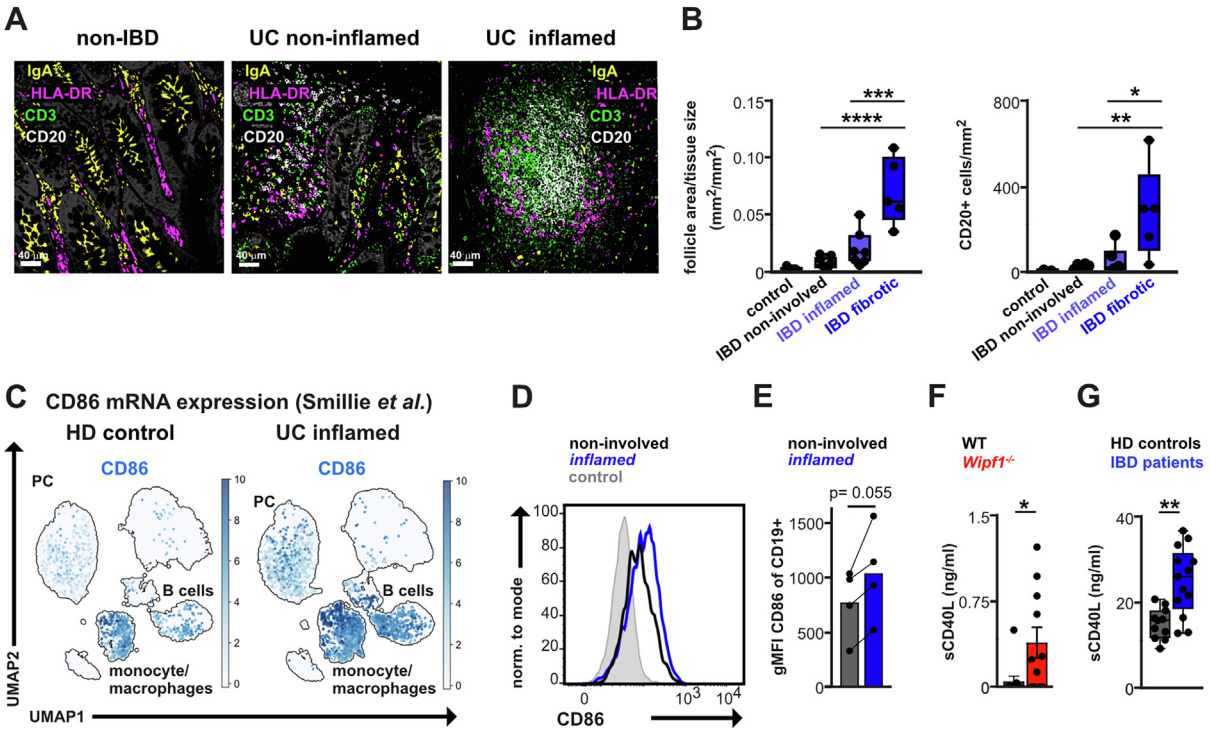

Fig. 6 B cells in inflamed intestinal tissue of IBD patients express elevated CD86. (A) Immunofluorescent microscopy of representative tissue sections of colonic tissue pieces of non-IBD patients or non-involved or inflamed tissue of UC patients stained for IgA plasma cells, CD3 T cells, CD20 B cells and HLA-DR <scale bars in µm>. (B) Automatically quantified follicle area/tissue size and CD20+ cells/mm^2 in immunohistochemical stainings of patient tissue sections and control tissue. (C) scRNA-seq analysis demonstrates significant upregulation of CD86 in colonic biopsies of inflamed UC patients compared to healthy tissue (data extracted from[33]). (D+E) Flow cytometry analysis of CD86 expression on ex vivo isolated CD20 expressing B cells isolated from non-involved and inflamed intestinal tissue of IBD patients (E) CD86 expression shown as gMFI. (F+G) sCD40L detected in sera of (F) WT or *Wipf1*$^{-/-}$ mice ($n \geq 10$ mice per genotype) or (G) HD or IBD patients ($n \geq 10$ sera per group). Statistical significance was calculated using (B) ordinary one-way analysis of variance with Tukey's multiple comparison test, (E) paired student's t test or (F+G) student's t test. *p < 0.05, **p < 0.01, ***p < 0.001, ****p < 0.0001. CD = clusters of differentiation; HD = healthy donor; IDB = inflammatory bowel disease; HLA = human leukocyte antigen; gMFI = geometric mean fluorescence intensity; ns = not significant; scRNA-seq = singe-cell RNA sequencing UC = ulcerative colitis; *Wipf1*$^{-/-}$ = Wiskott-Aldrich Syndrome interacting protein deficient; WT = wild type.

to systemic autoimmunity. Studies are underway to address this question.

Recent studies demonstrated that deleting CD80/CD86 on B cells abrogated spontaneous, splenic GCs in a mouse model of systemic lupus erythematosus (SLE), leading to reduced serum autoantibodies[37]. Here, we investigated whether using a CTLA-4-Ig as a treatment approach for intestinal inflammation in *Wipf1*$^{-/-}$ mice would have a similar effect. CTLA-4 is mainly expressed on activated and regulatory T cells and binds with high affinity to CD80/CD86 on antigen presenting cells, thereby preventing T cell costimulation. Recent data demonstrated that CD80/CD86 expression on B cells can be decreased by CTLA-4-Ig *in vitro*. *In vivo*, abatacept treatment of RA patients resulted in a sustained reduction of plasmablasts and serum IgG[22]. We here showed that blocking costimulatory signals through CTLA-4-Ig not only diminished aberrant humoral immune responses such as GC formation and the differentiation of IgG1-secreting intestinal ASCs but also inhibited the activation and priming of pro-inflammatory CD4 T cells. CTLA-4-Ig treatment reduced expression levels of CD86 on the surface of B cells isolated from mLN or colonic tissue. This could either be a direct effect through CTLA-4-Ig mediated downregulation as has been shown on human B cell line *in vitro*[22] or an indirect effect through decreased interaction with CD40L-providing CD4 T cells.

Interestingly, recently published scRNA-seq data comparing lymphocytes isolated from inflamed tissue biopsies of patients with UC to tissue biopsies of HD found a significant increase of CD86 mRNA in GC and follicular B cells[24]. In addition to B cell infiltration, we found CD86 protein levels also enhanced on B cells isolated from inflamed intestinal tissue of patients with IBD. Our data showed that CD86 is upregulated also on mouse WT B cells after LPS stimulation *in vitro* and was further enhanced by the presence of CD40L. CD40L is directly supplied by CD4 T cells during B/T interaction and promotes CSR to IgG. *In vivo*, we found elevated levels of sCD40L in the sera of *Wipf1*$^{-/-}$ mice as well as patients with IBD. Platelets have been described to express high levels of sCD40L in patients with WAS[38] and IBD[39], which correlated with the presence of autoantibodies as well as aberrant intestinal IgG production. sCD40L might locally elevate CD86 costimulation of B cells, thereby boosting aberrant B cell activation and CD4 T cell cytokine production. Thus, our data suggests that, in addition to the genetic predisposition for hyper-activation of B cells (such as in *Wipf1*$^{-/-}$ mice), the general inflammatory milieu (microbial components, sCD40L) pre-

sent during intestinal inflammation might trigger enhanced expression of the costimulatory molecule CD86 on activated B cells. Increased costimulation might then promote pro-inflammatory cytokine production of T cells. It was hypothesized that a UC-specific IFN-g expressing TfH cell subset could promote IgG CSR in active UC[3]. Albeit in a setting of genetically predisposed autoimmunity, our data provides a possible explanation for these observations, demonstrating that activated B cells directly induce IFN-g production by intestinal CD4 T cells and pointing at a crucial role for B/T interaction during intestinal inflammation. Although the level of B cell activation, the expression of costimulatory molecules (such as CD86), and their capacity of CD4 T-cell activation might vary considerably depending on the timepoint and the form of polygenic human IBD, our data points to a possible contribution of B cells to IBD pathology.

IBD therapy includes monoclonal antibody treatment against TNF-α and steroids; however, not all patients are responsive to these therapies. A small study analyzing B cell depletion in UC using rituximab has shown a possible short-term effect of mucosal healing which was not sustained[5]. However, rituximab treatment was well tolerated with no adverse effects in patients with UC. Rituximab treatment does not deplete gut-resident PC, which might provide one explanation for the lack of efficacy[40]. Likewise, abatacept treatment did not ameliorate symptoms in a small cohort of patients with CD or UC[41]. Our data suggests that depleting B cells or inhibiting costimulatory CD86 on B cells before the manifestation of disease and hence before the establishment of aberrant GC formation and IgG1 secreting ASC in intestinal tissues has the potential to put a (temporary) break on the vicious circle of intestinal inflammation. However, whether the initial B cell depletion in our mouse model of intestinal inflammation is sufficient or repetitive treatment is necessary remains to be determined. In this line, a recent study investigating B cell depletion in the pre-phase of a mouse model of SLE demonstrated that resetting the humoral immune system during the clinically unapparent phase alters immune homeostasis at later time points and delays systemic autoimmunity[42]. Defining reliable early biomarkers for IBD onset will be crucial for pre-disease treatment. Furthermore, recent data implicated that B cell accumulation during intestinal inflammation prevents the interaction between intestinal epithelial cells and stroma cells and delays mucosal healing[43]. Thus, B cell depletion in combination with other therapeutic interventions might also be beneficial to improve mucosal healing and achieve remission. Overall, our data suggests that the modulation of B cells during intestinal inflammatory diseases might add to the therapeutic options for the treatment of IBD.

METHODS

Mice

Wipf1$^{-/-}$ mice[44] were a kind gift from Raif Geha (Boston's Children Hospital, Boston, MA, USA), BALB/c WT, *RAG1*$^{-/-}$, C57BL/6 WT mice were bought from Charles River and bred at the Specific Opportunist Pathogen Free animal facility at the TranslaTUM. Igh-J^{tm1Dhu} mice (BALB/c JHT) mice were bought from Taconic Europe (Bomholtvej, Denmark). Female age-matched mice aged 6–12 weeks were used for all experiments. Littermate controls as well as cohoused mice were used whenever possible. All cages contained enrichment (houses, cotton rolls, wooden sticks) to reduce stress. For mixed-BM chimeras, 8–9 weeks old *RAG1*$^{-/-}$ recipients were irradiated with 2 × 4 Gy and injected intravenously the day after with a mixture of 80% BALB/c JHT with 20% WT or *Wipf1*$^{-/-}$ BM (4 × 10^6 BM cells in total). Repopulation was determined, and chimeras were used 8–10 weeks after injection. B cells were depleted from *Wipf1*$^{-/-}$ mice by *i.p.* administration of 250 µg/ml anti-CD20 (SA271G2, BioLegend, San Diego, CA, USA) or rat IgG2b, *k* Isotype control (RTK4530, BioLegend) at 6 weeks and 8 weeks of age, end analysis was performed at 10 weeks of age. To diminish CD86 costimulation, mice were treated with 25 mg/kg body weight of either CTLA-4-Ig (human/human, BE0099, Biozol, Eching, Germany) or human Fc-G1 (BE0096, Biozol). To induce colitis in *RAG1*$^{-/-}$ recipients, 5 × 10^5 sorted naive CD4 T cells (CD19$^-$CD4$^+$-CD25$^-$CD45RB^{hi}) were injected alone or in combination with MACS purified (purity more than 97%) 3 × 10^5 WT or *Wipf1*$^{-/-}$ B cells. Mice were monitored for weight loss and end analysis was performed 8 weeks post injection. Antibiotic treatment experiments were carried out on 6-week-old *Wipf1*−/− mice. Mice were given drinking water containing either 1% Glucose or 1% Glucose + Neomycinsulfat (1000 mg/g 2400515, belapharm) + Ampicillin-Trihydrat (1000 mg/g 1500561, belapharm) for 4 weeks and analyzed at 10 weeks of age. All mouse experiments were performed in accordance with the guidelines of the Federation of European Laboratory Animal Science Association and followed the legal approval of the Government of Upper Bavaria (Regierung von Oberbayern), Germany.

16s RNA sequencing

Fecal samples were collected from the cecum of non-cohoused WT and *Wipf1*$^{-/-}$ littermates. Total DNA from feces was isolated using the QiaAmp PowerFecal Pro DNA Kit on the QIAcube Connect device (Qiagen, Germantown, MD, USA). For 16S metagenomic analysis, variable regions V3 to V4 of the bacterial 16S ribosomal RNA gene were amplified by limited cycle polymerase chain reaction (PCR) and subjected to the Illumina 16S metagenomic sequencing library preparation workflow according to the manufacturer's recommendations (Illumina Inc., San Diego, CA, USA). The obtained DNA libraries were quantified, normalized, and pooled. After DNA library denaturation, samples were sequenced using MiSeq v3 sequencing chemistry with paired-end 300 bp reads on the Illumina MiSeq sequencer. Bioinformatic analysis (demultiplexing, primer/adapter/barcode removal, quality trimming, deficiency of adenosine deaminase 2 amplicon, classification, and composition analysis) was performed using the Qiime2 package[45]. Taxonomic classification was assigned by a native Bayes classifier trained on SILVA Database Rel. 132. Data visualization through 3D PCoA plots was performed using the Emperor tool. The Jaccard coefficient was calculated as a measure of the similarity of the gut microbiome composition (beta diversity) between WT and *Wipf1*$^{-/-}$ mice. Microbiome sequencing data were deposited in the European Nucleotide Archive under Project accession: PRJEB55760.

Quantitative PCR

Total RNA was extracted using the RNeasy Plus Mini or Micro Kit (Qiagen). Whole tissue RNA extraction was carried out using manual tissue disruption with Qiagen. RNA purity and concentration were measured using a NanoDrop spectrophotometer (Thermo Fisher Scientific, Dreieich, Germany) prior to cDNA synthesis using the High-Capacity cDNA Reverse Transcription Kit (Applied Biosystems/Thermo Fisher Scientific). qPCRs were carried out with the Takyon No ROX SYBR 2x MasterMix blue dTTP (Eurogentec, Seraing, Belgium) and the primers shown in

Supplementary Table 2 on the Light Cycler 480II (Roche, Basel, Switzerland) and gene expression were determined and normalized to *Hprt* using the $2^{-\Delta Ct}$ method.

Murine primary cell isolation and culture

Murine colons were collected, fat, and luminar contents carefully removed, tissue opened longitudinally and further cut into 0.5 cm pieces. Epithelial cell removal was carried out by incubating the tissue pieces in 10 mL pre-digestion medium [HBBS- Ca^{2+} and Mg^{2+} free, 10 mM 4-(2-hydroxyethyl)-1-piperazineethanesulfonic acid (HEPES) (Thermo Fisher Scientific), 5% fetal calf serum (FCS) (Thermo Fisher Scientific), 1x penicillin-streptomycin (P/S) (Invitrogen/Thermo Fisher Scientific), 5mM Ethylenediaminetetraacetic acid (EDTA) (Merck/Sigma-Aldrich, Darmstadt, Germany) and 1mM Dithiothreitol (DTT) (Sigma Aldrich) for 30 minutes rolling at 37°C. Prior to enzymatic digestion, the tissue pieces were washed by vortexing in 10 mL HBSS- Ca^{2+} and Mg^{2+} rich medium containing 10mM HEPES 1× P/S, and 5% FCS. Tissue samples were minced using scissors and incubated in 3 ml digestion medium [HBSS- Ca^{2+} and Mg^{2+} rich, 10mM HEPES, 1× P/S, 5% FCS, 0.5 mg/ml Collagenase D (Merck), 0.5 mg/ml DNase I (Merck) and 1 mg/ml Dispase II (Sigma Aldrich) for 30 minutes at 37°C on a thermal bloc. The cell/tissue suspension was mechanically dissociated, passed through a 100 µm cell strainer, lymphocytes purified through a Percoll (GE Healthcare, Solingen, Germany) gradient (25 minutes, 2200 rpm, 4°C, 1 acceleration, 0 deceleration), harvested at the 40/80% interface and washed in ice-cold B cell medium [RPMI-1640 + GlutaMax, 10mM HEPES, 10% FCS, 1× P/S and 0.05mM 2-Mercaptoethanol (Sigma Aldrich)]. MLN and spleen primary cells were harvested either by mechanical dissociation through a 70 µm cell strainer or enzymatic digestion in a digestion medium for 30 minutes at 37°C on a thermal bloc.

Splenic and mLN naove B cells were purified using negative B cell isolation kits yielding enriched populations of 95%–98% (Miltenyi Biotec, Bergisch Gladbach, Germany). Splenic naive CD4 T cells were purified using a negative naive CD4+ T-cell isolation Kit yielding a cell purity of 97%–99% (Miltenyi Biotec). For plasma cell differentiation, purified B cells were labeled in phosphate-buffered saline (PBS) with 1 µM CTV (Invitrogen) for 10 minutes at 37°C. Cells were maintained in a complete B cell medium. *In vitro* B and T-cell coculture systems were set up with 1×10^5 purified WT or *Wipf1*$^{-/-}$ B cells (BALB/c) and 2×10^5 purified WT naive CD4 T cells (C57BL/6). The cultures were stimulated with 5 µg/ml LPS (Sigma Aldrich) in B cell medium in the presence or absence of 10 µg/ml anti-CD86 (BioLegend), 1 µg/ml CD40L (Peprotech/Thermo Fisher Scientific), or 1µg/ml CTLA-4-Ig (human/human, BE0099, Biozol) for a total of 5 days.

Human samples

Informed, written consent was obtained from all patients and controls, with prior approval of the local ethics committee of the Faculty of Medicine of the Technical University of Munich (TUM), Germany, including two-fold pseudonymization for patient tissue and blood samples (TUM; #1926/2007, #5428/12 and 2022-297-S-KH). Blood samples were obtained from patients with IBD requiring diagnostic procedures or surgery. Control blood samples were obtained from healthy donors with no prior history of IBD or other autoimmune diseases. Tissue samples for histology were obtained from patients with IBD undergoing bowel resections of diseased bowel segments due to fibrotic intestinal obstruction or drug-resistant disease. Control tissue samples for histology were obtained from resection margins of surgical specimens from patients undergoing bowel resection surgery for cancer. Tissue sampling was performed in accordance with the regulations of the tissue bank of the TUM and Klinikum rechts der Isar, Munich.

Human primary cell isolation

Human colonic pieces of up to 1 g from UC or Crohn's Disease patients were obtained right after surgery from inflamed/fibrotic as well as uninvolved segments as declared by trained surgeons. Tissue pieces were washed in Ringer solution (Thermo Fisher Scientific) to remove blood clots and luminar contents by vortexing, and attached mesenteric adipose tissue was removed. The tissue was minced with scissors, and incubated in 5 ml digestion medium [HBSS [+]Ca^{2+} [+]Mg^{2+} with 3% BSA (Carl Roth, Karlsruhe, Germany), 10mM HEPES (Thermo Fisher Scientific), 5% FCS (Thermo Fisher Scientific), 1× P/S (Invitrogen), 2 Wünsch Units Liberase TL (Sigma Aldrich) and 0.5 mg/ml DNAseI (Merck)] on the GentleMACS (Miltenyi Biotech) in C Tubes (Miltenyi Biotech) with the preset 37C_h_TDK_1 program, filtered through a 100 µm mesh strainer and a 30%/80% Percoll gradient centrifugation was performed (25 minutes, 2200 rpm, 4°C, 1 acceleration, 0 deceleration). The lymphocyte-containing interface was manually pipetted off and washed with ice-cold gut cell medium [Opti-MEM (+)GlutaMAX with 10% FCS, 2.4 mg/ml sodium bicarbonate, 50uM 2-mercaptoethanol, 100 U/ml P/S] at 1200 rpm for 10 minutes.

Flow cytometric analysis

Single-cell suspensions were stained for viability using the Zombie Aqua fixable viability Kit (1:1000 BioLegend) and fixed with 4% paraformaldehyde (PFA) (VWR international/Sigma Aldrich). Cells were blocked with anti-mouse CD16/32 (93, 1:200, BioLegend) and CD16.2 (9E9, 1:200, BioLegend) followed by extracellular staining for 30 minutes with a combination of antibodies in Supplementary Table 3. For intracellular cytokine stainings, cells were cultured for 4 hours at 37°C in B cell medium containing 1× Cell Activation Cocktail (without Brefeldin A) (BioLegend) and 3 hours with 1× Protein Transporter Inhibitor Cocktail (Thermo Fisher Scientific). Post Live/Dead staining, cells were fixed, and permeabilized using the Intracellular Fixation and Permeabilization Buffer Set (Thermo Fisher Scientific) and stained with the appropriate combination of antibodies in Supplementary Table 3. Cells were acquired on LSR Fortessa cytometer (BD Biosciences, San Jose, California, US) and analyzed using FlowJo software (BD Biosciences). For flow sorting, murine splenic B cells (live $CD19^+B220^+$ cells) or naive CD4 T cells (live $CD19^-CD4^+CD25^-CD45RB^{hi}$ cells) were sorted on a FACSAria III (BD Biosciences) cell sorter.

Mass cytometry

A total of $3–5 \times 10^6$ cells per sample were stained for viability as described in Cell-ID Cisplatin (Standard BioTools, South San Francisco, California, US) with a final concentration of 2.5µM Cisplatin per sample, fixed in 2% Formaldehyde solution (w/v) methanol-free (Thermo Scientific Scientific) for 10 minutes at room temperature, washed 2x with Maxpar Cell Staining Buffer and left overnight at 4°C in 1 ml buffer. Cells were blocked with anti-mouse CD16/32 (93, 1:200, BioLegend) and CD16.2 (9E9, 1:200, BioLegend) followed by a surface staining with the combination of the antibodies listed in Supplementary Table 4 as described in Maxpar Cell Surface Staining (Standard BioTools). Intracellular

and intranuclear stainings were carried out as described in Maxpar Nuclear Antigen Staining with Fresh Fix (Standard BioTools) followed by a Cell-ID Intercalator-Ir staining (Standard BioTools) and sample prep for measurement on a CyTOF Helios with WB injector (Standard BioTools). The generated FCS files were normalized and randomized using EQ beads and concatenated. Clean-up gates for the elimination of no-cell signals, live cells, and single cells were conducted manually using FlowJo software (BD Bioscience). To balance the influence of markers with different dynamic ranges, we performed background subtraction and channel-based normalization. To identify distinct cell populations and clusters all markers were included in a two-round unbiased high-dimensional data analysis using the FlowJo plugins, FlowSOM, and Uniform Manifold Approximation and Projection.

Human colon single-cell RNA sequencing re-analysis

Annotated gene expression matrix of immune cells[24], (Single-Cell Portal: SCP259[3]; Gene Expression Omnibus GSE182270) were loaded, processed, and re-analyzed using the *scanpy* toolkit (version 1.9.1.[46]).

Low-quality observations, filtered individually per patient sample by number of genes (minimum: 200–600, maximum: 1800–3000) and percentage of mitochondrial genes (maximum.: 12%–20%) and genes expressed by fewer than three cells were removed (Supplementary Table 5). Gene counts were normalized to total counts per cell (target sum: 10^4), logarithmized, and scaled (maximum value: 10). To correct for batch effects, cells were integrated by unique samples using *harmonypy* (version 0.0.6.[47]), and Uniform Manifold Approximation and Projection for dimension reduction (nearest neighbors: 50, min. distance: 0.75, neg. edge sample rate: 9) was computed with the indicated settings.

Histology, Immunohistochemistry, Immunofluorescence

For histology, murine colons were flushed with ice-cold PBS, cut longitudinally, rolled, and fixed in 4% neutral buffered formalin for 48 hours, dehydrated, and embedded in paraffin (ASP 300S, Leica, Wetzlar, Germany) according to routine methods. Blocks were cut into 2 µm thick sections and stained with hematoxylin and eosin (H&E), or antibodies as indicated (CD3: clone SP7, DCS CI597R0, 1:100; B220: clone RA3-6B2, BD 550286, 1:50). IHC was performed on a Leica BondRxm using a Polymer Refine detection Kit with 3,3-diaminobenzidine as chromogen. All slides were scanned with a Leica AT2 scanning system with ×40 magnification and evaluated with ImageScope (12.4.0.7018). H&E-stained colon slides were analyzed and scored in an unbiased manner using the scoring scheme four (Supplementary Table 1, adapted from[16]). Colonic crypt length was determined by an average of 20 crypts per mouse gut roll using ImageJ. For immunofluorescence, murine colon rolls were fixed in 4%(w/v) PFA (VWR International), equilibrated in 30% (w/v) sucrose, and frozen at −80°C in Optimal Cutting Temperature embedding medium (Thermo Fischer Scientific). We then cut 20 µm sections, blocked in Blocking Buffer [PBS containing 1% (v/v) FCS, 1% (v/v) mouse serum (Jackson Immunoresearch, West Grove, Pennsylvania, US), 0.3% (v/v) Triton X-100] and stained with antibodies in Supplementary Table 6. Slides were washed in PBS, mounted with Fluoromount-G (Southern Biotech, Birmingham, Alabama, US), and sealed with a clear nail polish.

Human colon tissue samples were fixed in 4%(w/v) PFA (VWR International) for 24 hours at room temperature, dehydrated, embedded in paraffin, and cut into 3.5µm thick sections. Slides were deparaffinized, rehydrated, boiled in citrate buffer (10 mM pH6) for antigen retrieval, washed, and incubated in 50 mM NH_4Cl. Slides were blocked [2% BSA and 0.3% Triton X-100 (Sigma Aldrich)], labeled with a combination of the antibodies in Supplementary Table 6, and imaged using the Leica SP8 Confocal microscope or the Leica AT2 scanning system. For H&E and immunochemistry intestinal tissue was fixed in 4% PFA, dehydrated and paraffin-embedded. The sections were then stained with either standard H&E (Morphisto Ltd.) according to the manufacturer's instructions or with the antibody against CD20 (L26, Invitrogen), followed by a peroxidase-conjugated antibody (Jackson Immunoresearch) and 3,3-diaminobenzidine substrate chromogen Kit (Dako). Slides were scanned at 400x magnification (Aperio GT 450; Leica). CD20-positive cells were detected using QuPath software and its function for positive cell detection. In addition, CD20-positive follicles were counted, and their size measured.

Multiplex assays

Quantification of murine immunoglobulin and cytokines in blood serum, mucus scrapes, and culture supernatants was carried out using commercially available LEGENDplex Multiplex Assays (BioLegend), murine serum autoantibodies were quantified using the respective commercially available Alpha Diagnostics Intl. Kits and murine and human serum CD40L were quantified using the commercially available soluble CD40L ELISA Kits (Thermo Fisher Scientific), following the manufacturer's procedure.

Statistical analysis

Statistical analysis was performed with GraphPad Prism 7.0. The independent groups were compared at the explorative significance level of 5% and a power of 1-β = 80%. For independent samples t test were used for normally distributed continuous variables. In case of non-normality, the Mann-Whitney *U* test was used. A description of the statistical analysis of each graph can be found in the figure legends.

AUTHOR CONTRIBUTIONS

Conceptualization: SJK; Methodology: IG, JH, MG, SJK, JH, BB, OK, KS, PN, KJ; Investigation: IG, JH, MG, SJK, AB, MW, MK; Visualization: SJK, JH; Funding acquisition: SJK, JR; Project administration: SJK; Supervision: SJK; Writing – original draft: SJK; Writing – review & editing: SJK.

DECLARATION OF COMPETING INTERESTS

The authors have no competing interests to declare.

FUNDING

This work was supported by the German Research Foundation (DFG) grant Ke1737/2-1 (SJK), the Else-Kröner-Fresenius-Stiftung grant 2019_A105 (SJK), DFG grants (Project-ID 360372040–SFB 1335 and Project-ID 395357507–SFB 1371) awarded to KS, and DFG grants (Project-ID 210592381–SFB 1054, Project-ID 360372040–SFB 1335, Project-ID 395357507–SFB 1371, Project-ID 369799452–TRR 237, RU 695/9-1), and the European Research Council under the European Union's Horizon 2020 research and innovation program (grant agreement No 834154) awarded to JR.

DATA AVAILABILITY

The microbiome sequencing data referenced during the study are available in a public repository from the European Nucleotide Archive under the accession code PRJEB55760. All data supporting the findings of this study are available within the article and its Supplementary Information files and from the corresponding author upon reasonable request.

ACKNOWLEDGMENTS

We thank Raif Geha for providing *Wipf1*$^{-/-}$ mice and critical reading of the manuscript. We further thank Mark Boothby, Maike Hofmann, Julia Jellusova, Adam Wahida, Dieter Saur, Ari Waismann, and Nadine Hövelmeyer for valuable expertise, providing reagents, and critical reading of the manuscript. We thank the biological resource unit for animal husbandry (ZPF of the MRI at TUM), Konstanze Pechloff, and the core facility for flow cytometry (Ritu Mishra and Linda Bachmann) for excellent support. We further thank all members of the Institute for Clinical Chemistry and Pathobiochemistry for scientific discussions and support.

APPENDIX A. SUPPLEMENTARY DATA

Supplementary data to this article can be found online at https://doi.org/10.1016/j.mucimm.2023.10.005.

REFERENCES

1. Loftus Jr, E. V. Clinical epidemiology of inflammatory bowel disease: incidence, prevalence, and environmental influences. *Gastroenterology* **126**, 1504–1517 (2004).
2. Martin, J. C. et al. Single-cell analysis of Crohn's disease lesions identifies a pathogenic cellular module associated with resistance to anti-TNF therapy. *Cell* **178**, 1493–1508.e20 (2019).
3. Uzzan, M. et al. Ulcerative colitis is characterized by a plasmablast-skewed humoral response associated with disease activity. *Nat. Med.* **28**, 766–779 (2022).
4. Czarnewski, P. et al. Conserved transcriptomic profile between mouse and human colitis allows unsupervised patient stratification. *Nat. Commun.* **10**, 2892 (2019).
5. Leiper, K. et al. Randomised placebo-controlled trial of rituximab (anti-CD20) in active ulcerative colitis. *Gut* **60**, 1520–1526 (2011).
6. Eckmann, J. D. et al. De novo colitis associated with rituximab in 21 patients at a tertiary center. *Clin. Gastroenterol. Hepatol.* **18**, 252–253 (2020).
7. Cao, A. T. et al. Interleukin (IL)-21 promotes intestinal IgA response to microbiota. *Mucosal Immunol.* **8**, 1072–1082 (2015).
8. Burbage, M. & Keppler, S. J. Shaping the humoral immune response: actin regulators modulate antigen presentation and influence B-T interactions. *Mol. Immunol.* **101**, 370–376 (2018).
9. Macpherson, A., Khoo, U. Y., Forgacs, I., Philpott-Howard, J. & Bjarnason, I. Mucosal antibodies in inflammatory bowel disease are directed against intestinal bacteria. *Gut* **38**, 365–375 (1996).
10. Jostins, L. et al. Host-microbe interactions have shaped the genetic architecture of inflammatory bowel disease. *Nature* **491**, 119–124 (2012).
11. Tegtmeyer, D., Seidl, M., Gerner, P., Baumann, U. & Klemann, C. Inflammatory bowel disease caused by primary immunodeficiencies-Clinical presentations, review of literature, and proposal of a rational diagnostic algorithm. *Pediatr. Allergy Immunol.* **28**, 412–429 (2017).
12. Dupuis-Girod, S. et al. Autoimmunity in Wiskott-Aldrich syndrome: risk factors, clinical features, and outcome in a single-center cohort of 55 patients. *Pediatrics* **111**, e622–e627 (2003).
13. Curcio, C. et al. WIP null mice display a progressive immunological disorder that resembles Wiskott-Aldrich syndrome. *J. Pathol.* **211**, 67–75 (2007).
14. Nguyen, D. D. et al. Lymphocyte-dependent and Th2 cytokine-associated colitis in mice deficient in Wiskott-Aldrich syndrome protein. *Gastroenterology* **133**, 1188–1197 (2007).
15. Houston, S. A. et al. The lymph nodes draining the small intestine and colon are anatomically separate and immunologically distinct. *Mucosal Immunol.* **9**, 468–478 (2016).
16. Erben, U. et al. A guide to histomorphological evaluation of intestinal inflammation in mouse models. *Int. J. Clin. Exp. Pathol.* **7**, 4557–4576 (2014).
17. Keppler, S. J. et al. Wiskott-Aldrich syndrome interacting protein deficiency uncovers the role of the co-receptor CD19 as a generic hub for PI3 kinase signaling in B cells. *Immunity* **43**, 660–673 (2015).
18. Baumgart, D. C. & Sandborn, W. J. Crohn's disease. *Lancet* **380**, 1590–1605 (2012).
19. Danese, S. & Fiocchi, C. Ulcerative colitis. *N. Engl. J. Med.* **365**, 1713–1725 (2011).
20. Neurath, M. F. Cytokines in inflammatory bowel disease. *Nat. Rev. Immunol.* **14**, 329–342 (2014).
21. Ostanin, D. V. et al. T cell transfer model of chronic colitis: concepts, considerations, and tricks of the trade. *Am. J. Physiol. Gastrointest. Liver Physiol.* **296**, G135–G146 (2009).
22. Lorenzetti, R. et al. Abatacept modulates CD80 and CD86 expression and memory formation in human B-cells. *J. Autoimmun.* **101**, 145–152 (2019).
23. Ha, C. W. Y. et al. Translocation of viable gut microbiota to mesenteric adipose drives formation of creeping fat in humans. *Cell* **183**, 666–683.e17 (2020).
24. Smillie, C. S. et al. Intra- and inter-cellular rewiring of the human colon during ulcerative colitis. *Cell* **178**, 714–730.e22 (2019).
25. Yilmaz, B. et al. Microbial network disturbances in relapsing refractory Crohn's disease. *Nat. Med.* **25**, 323–336 (2019).
26. Gonçalves, P., Araújo, J. R. & Di Santo, J. P. A cross-talk between microbiota-derived short-chain fatty acids and the host mucosal immune system regulates intestinal homeostasis and inflammatory bowel disease. *Inflamm. Bowel Dis.* **24**, 558–572 (2018).
27. Luu, M. et al. The short-chain fatty acid pentanoate suppresses autoimmunity by modulating the metabolic-epigenetic crosstalk in lymphocytes. *Nat. Commun.* **10**, 760 (2019).
28. Biswas, A. et al. WASP-mediated regulation of anti-inflammatory macrophages is IL-10 dependent and is critical for intestinal homeostasis. *Nat. Commun.* **9**, 1779 (2018).
29. Choi, S. C. et al. Relative contributions of B cells and dendritic cells from lupus-prone mice to CD4+ T cell polarization. *J. Immunol.* **200**, 3087–3099 (2018).
30. Becker-Herman, S. et al. WASp-deficient B cells play a critical, cell-intrinsic role in triggering autoimmunity. *J. Exp. Med.* **208**, 2033–2042 (2011).
31. Recher, M. et al. B cell-intrinsic deficiency of the Wiskott-Aldrich syndrome protein (WASp) causes severe abnormalities of the peripheral B-cell compartment in mice. *Blood* **119**, 2819–2828 (2012).
32. Dahlberg, C. I. et al. Deletion of WASp and N-WASp in B cells cripples the germinal center response and results in production of IgM autoantibodies. *J. Autoimmun.* **62**, 81–92 (2015).
33. Kolhatkar, N. S. et al. B-cell intrinsic TLR7 signals promote depletion of the marginal zone in a murine model of Wiskott-Aldrich syndrome. *Eur. J. Immunol.* **45**, 2773–2779 (2015).
34. Arkatkar, T. et al. B cell-derived IL-6 initiates spontaneous germinal center formation during systemic autoimmunity. *J. Exp. Med.* **214**, 3207–3217 (2017).
35. Jackson, S. W. et al. B cell IFN-gamma receptor signaling promotes autoimmune germinal centers via cell-intrinsic induction of BCL-6. *J. Exp. Med.* **213**, 733–750 (2016).
36. Descatoire, M. et al. Critical role of WASp in germinal center tolerance through regulation of B cell apoptosis and diversification. *Cell Rep.* **38**:110474.
37. Chiang, K. et al. Cutting edge: A threshold of B cell costimulatory signals is required for spontaneous germinal center formation in autoimmunity. *J. Immunol.* **207**, 2217–2222 (2021).
38. Sereni, L. et al. Autonomous role of Wiskott-Aldrich syndrome platelet deficiency in inducing autoimmunity and inflammation. *J. Allergy Clin. Immunol.* **142**, 1272–1284 (2018).
39. Danese, S. et al. Activated platelets are the source of elevated levels of soluble CD40 ligand in the circulation of inflammatory bowel disease patients. *Gut* **52**, 1435–1441 (2003).
40. Uzzan, M. et al. Efficient long-term depletion of CD20+ B cells by rituximab does not affect gut-resident plasma cells. *Ann. N. Y. Acad. Sci.* **1415**, 5–10 (2018).
41. Sandborn, W. J. et al. Abatacept for Crohn's disease and ulcerative colitis. *Gastroenterology* **143**, 62–69.e4 (2012).
42. Werner, A. et al. Targeting B cells in the pre-phase of systemic autoimmunity globally interferes with autoimmune pathology. *iScience* **24**, 103076 (2021).
43. Frede, A. et al. B cell expansion hinders the stroma-epithelium regenerative cross talk during mucosal healing. *Immunity* **55**, 2336–2351.e12 (2022).
44. Antón, I. M. et al. WIP deficiency reveals a differential role for WIP and the actin cytoskeleton in T and B cell activation. *Immunity* **16**, 193–204 (2002).
45. Bolyen, E. et al. Reproducible, interactive, scalable and extensible microbiome data science using QIIME 2. *Nat. Biotechnol.* **37**, 852–857 (2019).
46. Wolf, F. A., Angerer, P. & Theis, F. J. SCANPY: large-scale single-cell gene expression data analysis. *Genome Biol.* **19**, 15 (2018).
47. Korsunsky, I. et al. Fast, sensitive and accurate integration of single-cell data with Harmony. *Nat. Methods* **16**, 1289–1296 (2019).